

000  
001  
002054  
055  
056003 

# External Prior Guided Internal Prior Learning for Real Noisy Image Denoising

057  
058004  
005  
006  
007  
008  
009  
010  
011059  
060  
061  
062  
063  
064  
065

012 Anonymous CVPR submission

066

013 Paper ID 1047

067

## Abstract

Most of existing image denoising methods use some statistical models such as additive white Gaussian noise (AWGN) to model the noise, and learn image priors from either external data or the noisy image itself to remove noise. However, the noise in real-world noisy images is much more complex than AWGN, and it is hard to be modeled by simple analytical distributions. Therefore, many state-of-the-art denoising methods in literature become much less effective when applied to real noisy images. In this paper, we develop a robust denoiser for real noisy image denoising without explicit assumption on noise models. Specifically, we first learn external priors from a set of clean natural images, and then use the learned external priors to guide the learning of internal latent priors from the given noisy image. The proposed method is simple yet highly effective. Experiments on real noisy images demonstrate that it achieves much better denoising performance than state-of-the-art denoising methods, including those designed for real noisy images.

## 1. Introduction

Image denoising is a crucial and indispensable step to improve image quality in digital imaging systems. In particular, with the decrease of size of CMOS/CCD sensors, noise is more easily to be corrupted and hence denoising is becoming increasingly important for high resolution imaging. In literature of image denoising, the observed noisy image is usually modeled as  $\mathbf{y} = \mathbf{x} + \mathbf{n}$ , where  $\mathbf{x}$  is the latent clean image and  $\mathbf{n}$  is the corrupted noise. Numerous image denoising methods [1, 2, 3, 4, 5, 6, 7, 8, 9, 10, 11, 12, 13] have been proposed in the past decades, including sparse representation and dictionary learning based methods [1, 2, 3], nonlocal self-similarity based methods [4, 5, 6, 3, 7], low-rank based methods [8], neural network based methods [9], and discriminative learning based methods [10, 11].

Most of the existing denoising methods [1, 2, 3, 4, 5, 6, 7, 8, 9, 10, 11, 12, 13] mentioned above assume noise  $\mathbf{n}$  to be additive white Gaussian noise (AWGN). Unfortunately, this assumption is too ideal to be true for real-world noisy im-

ages, where the noise is much more complex than AWGN [14, 15] and varies by different cameras and camera settings (ISO, shutter speed, and aperture, etc.). According to [15], the noise corrupted in the imaging process [is signal dependent and comes from five main sources: photon shot, fixed pattern, dark current, readout, and quantization noise. As a result, many advanced denoising methods in literature becomes much less effective when applied to real-world noisy images. Fig. 1 shows an example, where we apply some representative and state-of-the-art denoising methods, including CBM3D [6], WNNM [8], MLP [9], CSF [10], and TRD [11], to a real noisy image (captured by a Nikon D800 camera with ISO is 3200) provided in [14]. One can see that these methods either remain the noise or over-smooth the image details on this real noisy image.

There have been a few methods [14, 16, 17, 18, 19, 20, 21] developed for real noisy image denoising. Almost all of these methods follow a two-stage framework: first estimate the parameters of the assumed noise model (usually Gaussian or mixture of Gaussians (MoG)), and then perform denoising with the estimated noise model. Again, the noise in real noisy images is very complex and hard to be modeled by explicit distributions such as Gaussian and MoG. Fig. 1 also shows the denoised results of two state-of-the-art real noisy image denoising methods, Noise Clinic [19, 20] and Neat Image [21]. One can see that these two methods do not perform well on this noisy image either.

This work aims to develop a robust solution for real noisy image denoising without explicitly assuming certain noise models. To achieve this goal, we propose to first learn image priors from external clean images, and then employ the learned external priors to guide the learning of internal latent priors from the given noisy image. The flowchart of the proposed method is illustrated in Fig. 2. We first extract millions of patch groups from a set of high quality natural images, with which a Gaussian Mixture Model (GMM) is learned as the external prior. The learned GMM prior model is used to cluster the patch groups extracted from the given noisy image, and then a hybrid orthogonal dictionary (HOD) is learned as the internal prior for image denoising. Our proposed denoising method is simple and ef-

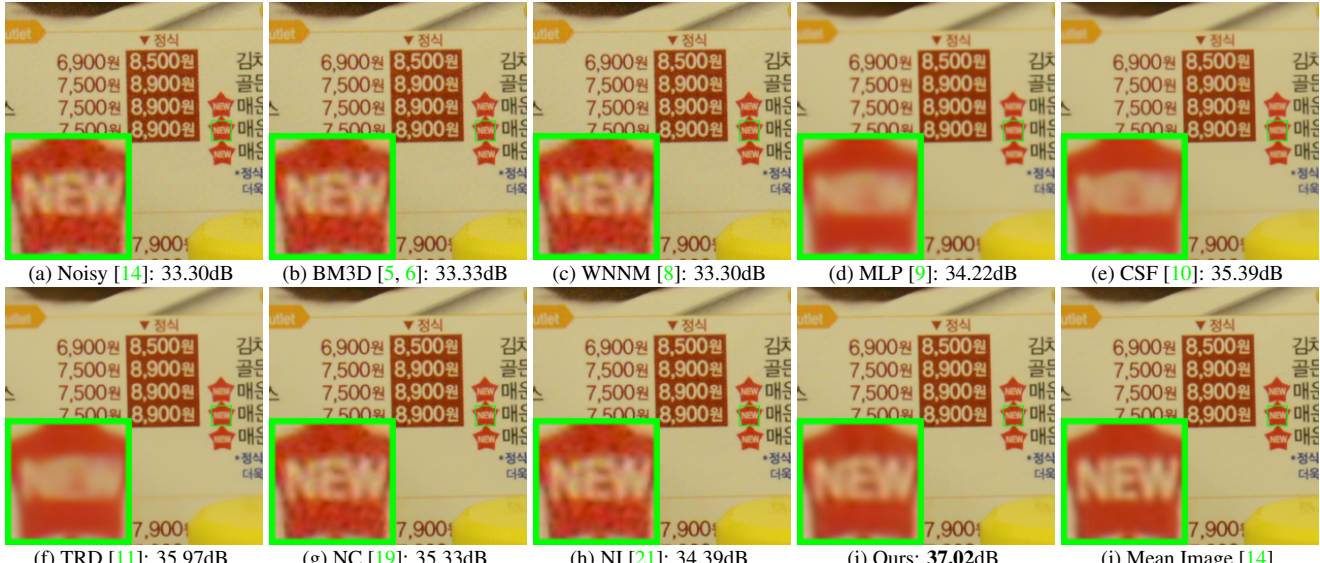


Figure 1. Denoised images of a noisy image cropped from the image “Nikon D800 ISO 3200 A3” from [14] by different methods. The images are better viewed by zooming in on screen.

ficient, yet our extensive experiments on real noisy images clearly demonstrate its better denoising performance than the current state-of-the-arts.

## 2. Related Work

### 2.1. Internal vs. External Prior Learning

Image priors are playing a key role in image denoising [7, 13, 1, 22, 3, 23]. There are mainly two categories of prior learning methods. 1) External prior learning methods [12, 7, 13] learn priors (e.g., dictionaries) from a set of external clean images, and the learned priors are used to recover the latent clean image from noisy images. 2) Internal prior learning methods [1, 3, 22, 23] directly learn priors from the given noisy image, and the image denoising is often done simultaneously with the prior learning process. It has been demonstrated [7, 13] that the external priors learned from natural clean images are effective and efficient for image denoising problem, but they are not adaptive to the given noisy image so that some fine-scale image structures may not be well recovered. By contrast, the internal priors are adaptive to content of the given image, but the learning processing are usually slow. In addition, most of the internal prior learning methods [1, 3, 22, 23] assume AWGN noise, making the learned priors less robust for real noisy images. In this paper, we use external priors to guide the internal prior learning. Our method is not only much faster than the traditional internal learning methods, but also very effective to denoise real noisy images.

### 2.2. Real Noisy Image Denoising

Recently, several image denoising methods [16, 17, 19, 20, 18, 14] are proposed to remove unknown noise. These

methods can be directly applied to denoise real noisy images. Among them, the “Noise Clinic” [19, 20] estimated the noise by a multivariate Gaussian and remove the noise by a generalized version of nonlocal Bayesian model [24]. Zhu *et al.* proposed a Bayesian method [18] to approximate and remove the noise via a low-rank MoG model. There are also several methods developed specifically for real noisy image denoising [14, 21]. The [14] modeled the cross-channel noise in real noisy image as a multivariate Gaussian and the noise is removed by Bayesian nonlocal means. The commercial software Neat Image [21] estimated the noise parameters from a flat region of the given noisy image and filtered the noise correspondingly. Almost all these methods [16, 17, 19, 20, 18, 14] use Gaussian or mixture of Gaussians (MoG) to model the noise in real noisy images. However, the noise in real noisy images is very complex and hard to be modeled by explicit distributions.

## 3. External Prior Guided Internal Prior Learning

In this section, we first describe the learning of external prior, and then describe in detail the guided internal prior learning. Finally, the denoising algorithm with the learned priors is presented.

### 3.1. Learn External Patch Group Priors

The nonlocal self-similarity based patch group (PG) [7] has proved to be a very effective unit for image prior learning. In this work, we also extract PGs from natural clean images to learn priors. A PG is a group of similar patches to a local patch.

In our method, each local patch is extracted from a

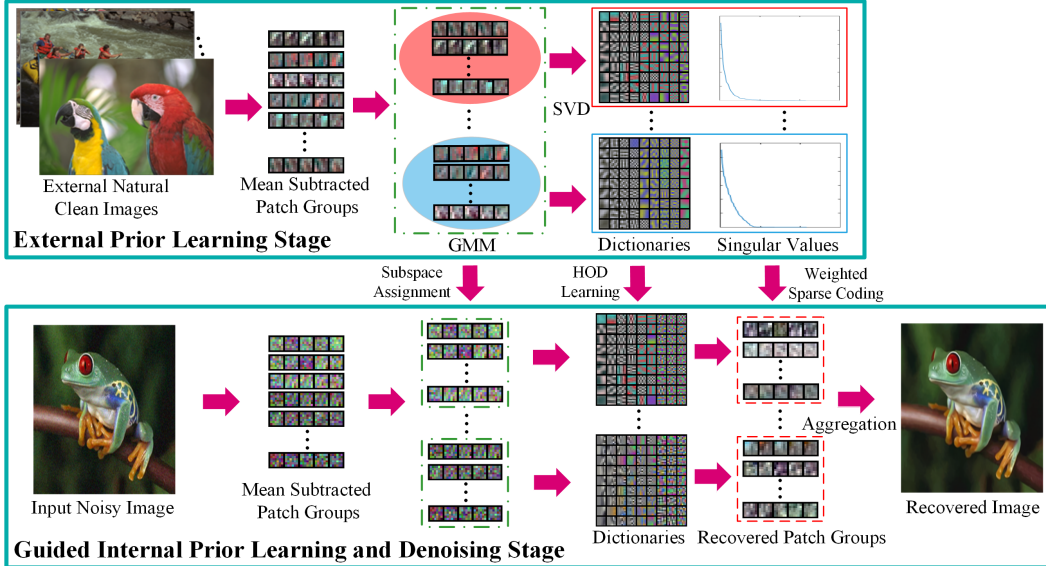


Figure 2. Flowchart of the proposed external prior guided internal prior learning and real noisy image denoising framework.

RGB image with patch size  $p \times p \times 3$ . We search the  $M$  most similar patches to this local patch (including the local patch itself) in a  $W \times W$  local region around it. Each patch is stretched to a patch vector  $\mathbf{x}_m \in \mathbb{R}^{3p^2 \times 1}$  to form the PG  $\{\mathbf{x}_m\}_{m=1}^M$ . The mean vector of this PG is  $\boldsymbol{\mu} = \frac{1}{M} \sum_{m=1}^M \mathbf{x}_m$ , and the group mean subtracted PG is defined as  $\bar{\mathbf{X}} \triangleq \{\bar{\mathbf{x}}_m = \mathbf{x}_m - \boldsymbol{\mu}\}$ .

Assume we extract a number of  $N$  PGs from a set of external natural images, and the  $n$ -th PG is  $\bar{\mathbf{X}}_n \triangleq \{\bar{\mathbf{x}}_{n,m}\}_{m=1}^M, n = 1, \dots, N$ . A Gaussian Mixture Model (GMM) is learned to model the PG prior. The overall log-likelihood function is

$$\ln \mathcal{L} = \sum_{n=1}^N \ln \left( \sum_{k=1}^K \pi_k \prod_{m=1}^M \mathcal{N}(\bar{\mathbf{x}}_{n,m} | \boldsymbol{\mu}_k, \boldsymbol{\Sigma}_k) \right). \quad (1)$$

The learning process is similar to the GMM learning in [7, 13]. Finally, a GMM model with  $K$  Gaussian components is learned, and the learned parameters include mixture weights  $\{\pi_k\}_{k=1}^K$ , mean vectors  $\{\boldsymbol{\mu}_k\}_{k=1}^K$ , and covariance matrices  $\{\boldsymbol{\Sigma}_k\}_{k=1}^K$ . Note that the mean vector of each cluster is naturally zero, i.e.,  $\boldsymbol{\mu}_k = \mathbf{0}$ .

To better describe the subspace of each Gaussian component, we perform singular value decomposition (SVD) on the covariance matrix:

$$\boldsymbol{\Sigma}_k = \mathbf{U}_k \mathbf{S}_k \mathbf{U}_k^\top. \quad (2)$$

The eigenvector matrices  $\{\mathbf{U}_k\}_{k=1}^K$  will be employed as the external orthogonal dictionary to guide the internal dictionary learning in next sub-section. The singular values in  $\mathbf{S}_k$  reflect the significance of the singular vectors in  $\mathbf{U}_k$ . They will also be utilized as prior weights for weighted sparse coding in our denoising algorithm.

### 3.2. Guided Internal Prior Learning

After the external PG prior is learned, we employ it to guide the internal PG prior learning for a given real noisy

image. The guidance lies in two aspects. One is that the external prior can guide the subspace assignment of internal noisy PGs, while the other is that the external prior could guide the orthogonal dictionary learning of internal noisy PGs.

#### 3.2.1 Internal Subspace Assignment

Given a real noisy image  $\mathbf{y}$ , we extract  $N$  (overlapped) local patches from it. Similar to the external prior learning stage, for the  $n$ -th local patch we search its  $M$  most similar patches around it to form a noisy PG, denoted by  $\mathbf{Y}_n = \{\mathbf{y}_{n,1}, \dots, \mathbf{y}_{n,M}\}$ . Then the group mean of  $\mathbf{Y}_n$ , denoted by  $\boldsymbol{\mu}_n$ , is subtracted from each patch by  $\bar{\mathbf{y}}_{n,m} = \mathbf{y}_{n,m} - \boldsymbol{\mu}_n$ , leading to the mean subtracted noisy PG  $\bar{\mathbf{Y}}_n \triangleq \{\bar{\mathbf{y}}_{n,m}\}_{m=1}^M$ .

The external GMM prior models  $\{\boldsymbol{\Sigma}_k\}_{k=1}^K$  basically characterize the subspaces of natural high quality PGs. Therefore, we project the noisy PG  $\bar{\mathbf{Y}}_n$  into the subspaces of  $\{\boldsymbol{\Sigma}_k\}_{k=1}^K$  and assign it to the most suitable subspace based on the posterior probability:

$$P(k|\bar{\mathbf{Y}}_n) = \frac{\prod_{m=1}^M \mathcal{N}(\bar{\mathbf{y}}_{n,m} | \mathbf{0}, \boldsymbol{\Sigma}_k)}{\sum_{l=1}^K \prod_{m=1}^M \mathcal{N}(\bar{\mathbf{y}}_{n,m} | \mathbf{0}, \boldsymbol{\Sigma}_l)} \quad (3)$$

for  $k = 1, \dots, K$ . Then  $\bar{\mathbf{Y}}_n$  is assigned to the component with the maximum A-posteriori (MAP) probability  $\max_k P(k|\bar{\mathbf{Y}}_n)$ .

#### 3.2.2 Guided Orthogonal Dictionary Learning

Assume we have assigned all the internal noisy PGs  $\{\bar{\mathbf{Y}}_n\}_{n=1}^N$  to their corresponding most suitable subspaces in  $\{\mathcal{N}(\mathbf{0}, \boldsymbol{\Sigma}_k)\}_{k=1}^K$ . For the  $k$ -th subspace, the noisy PGs assigned to it are  $\{\bar{\mathbf{Y}}_{k,n}\}_{n=1}^{N_k}$  where  $\bar{\mathbf{Y}}_{k,n} = [\bar{\mathbf{y}}_{k,n,1}, \dots, \bar{\mathbf{y}}_{k,n,M}]$

and  $\sum_{k=1}^K N_k = N$ . We propose to learn an orthogonal dictionary  $\mathbf{D}_k$  from each set of PGs  $\bar{\mathbf{Y}}_{k,n}$  to characterize the internal PG prior with the guidance of the corresponding external orthogonal dictionary  $\mathbf{U}_k$  (Eq. (2)). The reasons that we learn orthogonal dictionaries are two-fold. Firstly, the PGs  $\bar{\mathbf{Y}}_{k,n}$  are in a subspace of the whole space of all PGs, therefore, there is no necessary to learn a redundant over-complete dictionary to characterize it, while an orthonormal dictionary has naturally zero *mutual incoherence* [25]. Secondly, the orthogonality of dictionary can make the encoding in the testing stage very efficient, leading to an efficient denoising algorithm (please refer to sub-section 3.3 for details).

We let the orthogonal dictionary  $\mathbf{D}_k$  be  $\mathbf{D}_k \triangleq [\mathbf{D}_{k,E} \mathbf{D}_{k,I}] \in \mathbb{R}^{3p^2 \times 3p^2}$ , where  $\mathbf{D}_{k,E} = \mathbf{U}_k(:, 1:r) \in \mathbb{R}^{3p^2 \times r}$  is the external sub-dictionary and it includes the first  $r$  most important eigenvectors of  $\mathbf{U}_k$ , and the internal sub-dictionary  $\mathbf{D}_{k,I}$  is to be adaptively learned from the noisy PGs  $\{\bar{\mathbf{Y}}_{k,n}\}_{n=1}^{N_k}$ . The rationale to design  $\mathbf{D}_k$  as a hybrid dictionary is as follows. The external sub-dictionary  $\mathbf{D}_{k,E}$  is pre-trained from external clean data, and it represents the  $k$ -th latent subspace of natural images, which is helpful to reconstruct the common latent structures of images. However,  $\mathbf{D}_{k,E}$  is general to all images and it is not adaptive to the given noisy image. Some fine-scale details specific to the given image may not be well characterized by  $\mathbf{D}_{k,E}$ . Therefore, we learn an internal sub-dictionary  $\mathbf{D}_{k,I}$  to supplement  $\mathbf{D}_{k,E}$ . In other words,  $\mathbf{D}_{k,I}$  is to reveal the latent subspace adaptive to the input noisy image, which cannot be effectively represented by  $\mathbf{D}_{k,E}$ .

For notation simplicity, in the following development we ignore the subspace index  $k$  for  $\bar{\mathbf{Y}}_{k,n}$  and  $\mathbf{D}_k$ , etc. The learning of hybrid orthogonal dictionary  $\mathbf{D}$  is performed under the following weighted sparse coding framework:

$$\begin{aligned} & \min_{\mathbf{D}_I, \{\alpha_{n,m}\}} \sum_{n=1}^N \sum_{m=1}^M (\|\bar{\mathbf{y}}_{n,m} - \mathbf{D}\alpha_{n,m}\|_2^2 + \sum_{j=1}^{3p^2} \lambda_j |\alpha_{n,m,j}|) \\ & \text{s.t. } \mathbf{D} = [\mathbf{D}_E \mathbf{D}_I], \mathbf{D}_I^\top \mathbf{D}_I = \mathbf{I}_r, \mathbf{D}_E^\top \mathbf{D}_I = \mathbf{0}, \end{aligned} \quad (4)$$

where  $\alpha_{n,m}$  is the sparse coding vector of the  $m$ -th patch  $\bar{\mathbf{y}}_{n,m}$  in the  $n$ -th PG  $\bar{\mathbf{Y}}_n$  and  $\alpha_{n,m,j}$  is the  $j$ -th element of  $\alpha_{n,m}$ .  $\lambda_j$  is the  $j$ -th regularization parameter defined as

$$\lambda_j = \lambda / (\sqrt{\mathbf{S}_k(j)} + \varepsilon), \quad (5)$$

where  $\mathbf{S}_k(j)$  is the  $j$ -th singular value of diagonal singular value matrix  $\mathbf{S}_k$  (please refer to Eq. (2)) and  $\varepsilon$  is a small positive number to avoid zero denominator. Noted that  $\mathbf{D}_E = \mathbf{U}_k$  if  $r = 3p^2$  and  $\mathbf{D}_E = \emptyset$  if  $r = 0$ . The dictionary  $\mathbf{D} = [\mathbf{D}_E \mathbf{D}_I]$  is orthogonal by checking that:

$$\mathbf{D}^\top \mathbf{D} = \begin{bmatrix} \mathbf{D}_E^\top \\ \mathbf{D}_I^\top \end{bmatrix} [\mathbf{D}_E \mathbf{D}_I] = \begin{bmatrix} \mathbf{D}_E^\top \mathbf{D}_E & \mathbf{D}_E^\top \mathbf{D}_I \\ \mathbf{D}_I^\top \mathbf{D}_E & \mathbf{D}_I^\top \mathbf{D}_I \end{bmatrix} = \mathbf{I} \quad (6)$$

We employ an alternating iterative approach to solve the optimization problem (4). Specifically, we initialize the orthogonal dictionary as  $\mathbf{D}^{(0)} = \mathbf{U}_k$  and for  $t = 0, 1, \dots, T-1$ , we alternatively update  $\alpha_{n,m}$  and  $\mathbf{D}$  as follows:

**Updating Sparse Coefficient:** Given the orthogonal dictionary  $\mathbf{D}^{(t)}$ , we update each sparse coding vector  $\alpha_{n,m}$  by solving

$$\alpha_{n,m}^{(t)} := \arg \min_{\alpha_{n,m}} \|\bar{\mathbf{y}}_{n,m} - \mathbf{D}^{(t)} \alpha_{n,m}\|_2^2 + \sum_{j=1}^{3p^2} \lambda_j |\alpha_{n,m,j}| \quad (7)$$

Since dictionary  $\mathbf{D}^{(t)}$  is orthogonal, the problems (7) has a closed-form solution

$$\alpha_{n,m}^{(t)} = \text{sgn}((\mathbf{D}^{(t)})^\top \bar{\mathbf{y}}_{n,m}) \odot \max(|(\mathbf{D}^{(t)})^\top \bar{\mathbf{y}}_{n,m}| - \boldsymbol{\lambda}, \mathbf{0}), \quad (8)$$

where  $\boldsymbol{\lambda} = [\lambda_1, \lambda_2, \dots, \lambda_{3p^2}]$  is the vector of regularization parameter and  $\text{sgn}(\bullet)$  is the sign function,  $\odot$  means element-wise multiplication. The detailed derivation of Eq. (8) can be found in the supplementary file.

**Updating Internal Sub-dictionary:** Given the sparse coding vectors  $\{\alpha_{n,m}^{(t)}\}$ , we update the internal sub-dictionary by solving

$$\begin{aligned} \mathbf{D}_I^{(t+1)} &:= \arg \min_{\mathbf{D}_I} \sum_{n=1}^N \sum_{m=1}^M (\|\bar{\mathbf{y}}_{n,m} - \mathbf{D}_I \alpha_{n,m}^{(t)}\|_2^2) \\ &= \arg \min_{\mathbf{D}_I} \|\mathbf{Y} - \mathbf{D} \mathbf{A}^{(t)}\|_F^2 \end{aligned} \quad (9)$$

$$\text{s.t. } \mathbf{D} = [\mathbf{D}_E \mathbf{D}_I], \mathbf{D}_I^\top \mathbf{D}_I = \mathbf{I}_r, \mathbf{D}_E^\top \mathbf{D}_I = \mathbf{0},$$

where  $\mathbf{A}^{(t)} = [\alpha_{1,1}^{(t)}, \dots, \alpha_{1,M}^{(t)}, \dots, \alpha_{N,1}^{(t)}, \dots, \alpha_{N,M}^{(t)}]$ . The sparse coefficient matrix can be written as  $\mathbf{A}^{(t)} = [(\mathbf{A}_E^{(t)})^\top (\mathbf{A}_I^{(t)})^\top]^\top$  where the external part  $\mathbf{A}_E^{(t)} \in \mathbb{R}^{r \times NM}$  and the internal part  $\mathbf{A}_I^{(t)} \in \mathbb{R}^{(3p^2-r) \times NM}$  represent the coding coefficients of  $\mathbf{Y}$  over external sub-dictionary  $\mathbf{D}_E$  and internal sub-dictionary  $\mathbf{D}_I$ , respectively. According to the Theorem 4 in [26], the problem (9) has a closed-form solution  $\mathbf{D}_I^{(t+1)} = \mathbf{U}_I \mathbf{V}_I^\top$ , where  $\mathbf{U}_I \in \mathbb{R}^{3p^2 \times r}$  and  $\mathbf{V}_I \in \mathbb{R}^{r \times r}$  are the orthogonal matrices obtained by the following SVD

$$(\mathbf{I} - \mathbf{D}_E \mathbf{D}_E^\top) \mathbf{Y} (\mathbf{A}_I^{(t)})^\top = \mathbf{U}_I \mathbf{S}_I \mathbf{V}_I^\top. \quad (10)$$

The orthogonality of internal dictionary  $\mathbf{D}_I^{(t+1)}$  can be checked by  $(\mathbf{D}_I^{(t+1)})^\top (\mathbf{D}_I^{(t+1)}) = \mathbf{V}_I \mathbf{U}_I^\top \mathbf{U}_I \mathbf{V}_I^\top = \mathbf{I}_r$ .

### 3.3. The Denoising Algorithm

The denoising of the given noisy image  $\mathbf{y}$  can be simultaneously done with the guided internal dictionary learning process. Once we obtain the solutions of sparse coding vectors  $\{\hat{\alpha}_{n,m}^{(T-1)}\}$  in Eq. (8) and the orthogonal dictionary  $\mathbf{D}^{(T)} = [\mathbf{D}_E \mathbf{D}_I^{(T)}]$  in Eq. (9), the latent clean patch of a noisy patch  $\hat{\mathbf{y}}_{n,m}$  in PG  $\mathbf{Y}_n$  is reconstructed as

432   **Alg. 1:** External Prior Guided Internal Prior Learning  
 433    for Real Noisy Image Denoising

434   **Input:** Noisy image  $y$ , external PG prior GMM model  
 435   **Output:** The denoised image  $\hat{x}$ .  
 436   **Initialization:**  $\hat{x}^{(0)} = y$ ;  
 437   **for**  $Ite = 1 : IteNum$  **do**  
 438     1. Extracting internal PGs from  $\hat{x}^{(Ite-1)}$ ;  
 439       **for** each PG  $\mathbf{Y}_n$  **do**  
 440         2. Calculate group mean vector  $\mu_n$  and form  
 441           mean subtracted PG  $\bar{\mathbf{Y}}_n$ ;  
 442         3. Subspace assignment via Eq. (3);  
 443       **end for**  
 444       **for** the PGs in each Subspace **do**  
 445         4. External PG prior Guided Internal Orthogonal  
 446           Dictionary Learning by solving (4);  
 447         5. Recover each patch in all PGs via Eq. (11);  
 448       **end for**  
 449       6. Aggregate the recovered PGs of all subspaces to form  
 450           the recovered image  $\hat{x}^{(Ite)}$ ;  
 451   **end for**

$$\hat{y}_{n,m} = \mathbf{D}^{(T)} \hat{\alpha}_{n,m} + \mu_n, \quad (11)$$

452  
 453  
 454  
 455  
 456 where  $\mu_n$  is the group mean of  $\mathbf{Y}_n$ . The latent clean image  
 457 is then reconstructed by aggregating all the reconstructed  
 458 patches in all PGs. We perform the above denoising pro-  
 459 cedures for several iterations for better denoising outputs.  
 460 The proposed denoising algorithm is summarized in Alg. 1.  
 461 The latent clean image  $\hat{x}$  is reconstructed by aggregating all  
 462 the estimated PGs. Similar to [7], we perform the above  
 463 denoising procedures for several iterations for better denoising  
 464 outputs. The proposed denoising algorithm is summarized  
 465 in Alg. 1.

## 4. Experiments

466 We evaluate the performance of the proposed algorithm  
 467 on real-world noisy images [14, 20] in comparison with  
 468 state-of-the-art denoising methods [5, 6, 9, 8, 10, 11, 14,  
 469 19, 20, 21].

### 4.1. Implementation Details

470 Our proposed method has two stages: the external prior  
 471 learning stage and the external prior guided internal prior  
 472 learning stage. In the first stage, we set  $p = 6$  (the patch  
 473 size),  $M = 10$  (the number of similar patches in a PG),  
 474  $W = 31$  (the window size for PG searching) and  $K =$   
 475 32 (the number of Gaussian components in GMM. We  
 476 learn the external GMM prior with 3.6 million PGs ex-  
 477 tracted from the Kodak PhotoCD Dataset (<http://r0k.us/graphics/kodak/>), which includes 24 high quality  
 478 color images.

479 In the second stage, we set  $r = 54$  (the number of atoms  
 480 in the external sub-dictionaries); that is, we let the external



481 Figure 3. Some samples cropped from real noisy images of [14].

482 sub-dictionary have the same number of atoms as the inter-  
 483 nal sub-dictionary to be learned. Our experiments show that  
 484 setting  $r$  between 27 and 81 will lead to very similar results.  
 485 For other parameters, we set  $\lambda = 0.001$  (the sparse regu-  
 486 larization parameter),  $T = 2$  (the number of iterations for  
 487 solving problem (4)), and  $IteNum = 4$  (the number of iter-  
 488 ations for Alg.1). All parameters of our method are fixed to  
 489 all experiments, which are run under the Matlab2014b en-  
 490 vironment on a machine with Intel(R) Core(TM) i7-5930K  
 491 CPU of 3.5GHz and 32GB RAM.

### 4.2. The Testing Datasets

492 We evaluate the proposed method on two real noisy im-  
 493 ages datasets, where the images were captured under indoor  
 494 or outdoor lighting conditions by different types of cameras  
 495 and camera settings.

496 The first dataset is provided in [20], which includes 20  
 497 real noisy images collected under uncontrolled outdoor en-  
 498 vironment. Since there is no “ground truth” of the noisy im-  
 499 ages, the objective measures such as PSNR cannot be com-  
 500 puted on this dataset.

501 The second dataset is provided in [14], which includes  
 502 noisy images of 17 static scenes. The noisy images were  
 503 collected under controlled indoor environment. Each scene  
 504 was shot 500 times under the same camera and camera set-  
 505 ting. The mean image of the 500 shots is roughly taken as  
 506 the “ground truth”, with which the PSNR can be computed.  
 507 Since the image size is very large (about  $7000 \times 5000$ ) and  
 508 the 17 scenes share repetitive contents, the authors of [14]  
 509 cropped 15 smaller images (of size  $512 \times 512$ ) to perform  
 510 experiments. To more comprehensively evaluate the pro-  
 511 posed methods, we cropped 60 images of size  $500 \times 500$   
 512 from the dataset for experiments. Some samples are shown  
 513 in Fig. 3. Note that the noise in our cropped 60 images is  
 514 different from the noise in the 15 images cropped by the  
 515 authors of [14] since they are from different shots.

### 4.3. Comparison among external, internal and guided internal priors

516 To demonstrate the advantages of external prior guided  
 517 internal priors, in this section we perform real noisy image  
 518 denoising by using external priors (denoted by “External”),  
 519 internal priors (denoted by “Internal”), and the proposed  
 520 guided internal priors (denoted by “Guided Internal”), re-  
 521 spectively. For the “External” method, we utilize the full  
 522 external dictionaries (i.e.,  $r = 108$  in Eq. (4)) for denois-  
 523 ing.

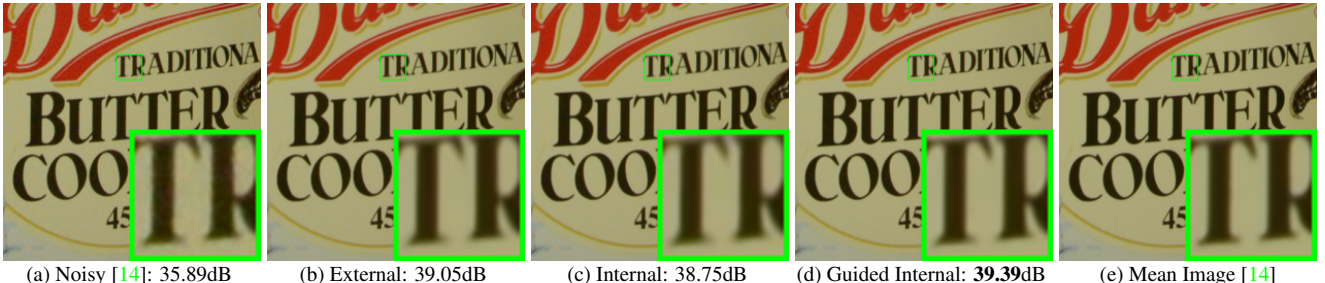


Figure 4. Denoised images of a noisy image cropped from the image “Nikon D600 ISO 3200 C1” [14] by different methods. The images are better to be zoomed in on screen.

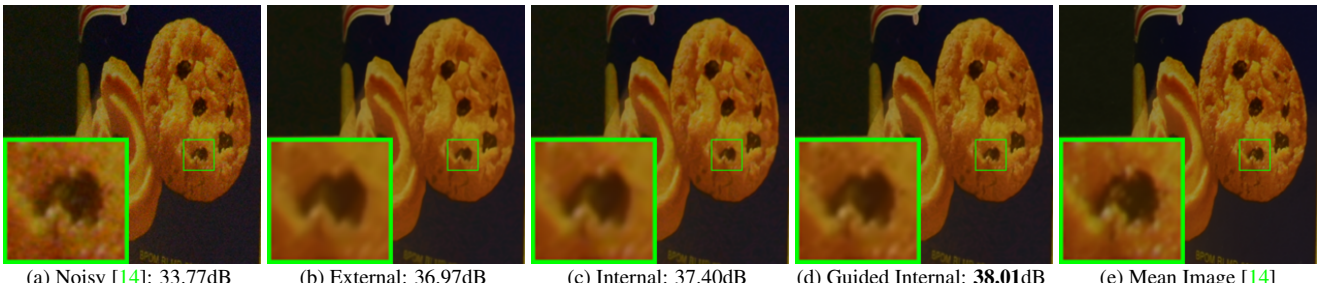


Figure 5. Denoised images of a noisy image cropped from the image “Nikon D600 ISO 3200 C1” [14] by different methods. The images are better to be zoomed in on screen.

Table 1. Average PSNR (dB) results and Run Time (seconds) of the External, the Internal, and our proposed methods on 60 real noisy images (of size  $500 \times 500 \times 3$ ) cropped from [14].

|      | Noisy | External     | Internal | Guided Internal |
|------|-------|--------------|----------|-----------------|
| PSNR | 34.51 | 38.21        | 38.07    | <b>38.75</b>    |
| Time | —     | <b>39.57</b> | 587.36   | 41.89           |

ing. For the “Internal” method, the overall framework is similar to the method of [3]. A GMM model (with  $K = 32$  Gaussians) is directly learned from the PGs extracted from the given noisy image without using any external data, and then the internal orthogonal dictionary is obtained via Eqn. (2) to perform denoising. All parameters of the “External” and “Internal” methods are tuned to achieve their best performance.

We compare the three methods mentioned above on the 60 cropped images from [14]. The average PSNR and run time are listed in Table 1. It can be seen that “Guided Internal” prior achieves better PSNR than both “External” and “Internal” priors. In addition, the “Internal” method is very slow because it involves online GMM learning, while the “Guided Internal” method is only a little slower than the “External” method. Fig. 4 and Fig. 5 show the denoised images of two noisy image by the three methods. We can see that the “External” method is good at recovering large-scale structures (see Fig. 4) while the “Internal” method is good at recovering fine-scale textures (see Fig. 5). By utilizing external priors to guide the internal prior learning, our proposed method can effectively recover both the large-scale structures and fine-scale textures.

#### 4.4. Comparison with State-of-the-Art Denoising Methods

We compare the proposed method with state-of-the-art image denoising methods, including CBM3D [5, 6], WNNM [8], MLP [9], CSF [10], TNRD [11], Noise Clinic (NC) [19], Cross-Channel (CC) [14], and Neat Image (NI) [21]. Among them, CBM3D, WNNM, MLP, CSF and TNRD are designed based on Gaussian noise model, and they need to know the noise level for denoising. We use the method in [27] to estimate the noise level for them. All the other parameters in these methods are set as the default ones. Since WNNM, MLP, CSF and TNRD are designed for grayscale images, we use them to denoise the R, G, B channels separately for color noisy images.

Like our method, the NC is a blind image denoising method which does not need any noise prior. The NI is a commercial software for image denoising, which has been embedded into Photoshop and Corel PaintShop [21]. The code of CC is not released but its results on the 15 cropped images are available at [14]. Therefore, we only compare with it on the 15 cropped images from [14].

##### 4.4.1 Results on Dataset [20]

Since there is no “ground truth” for the real noisy images in dataset [20], we only compare the visual quality of the denoised images by different methods. (Note that method CC [14] is not compared since its code is not available.) Fig. 7 shows the denoised images of “Dog”. It can be seen that CBM3D and WNNM tend to over-smooth much the image while remaining some noise caused color artifacts. MLP

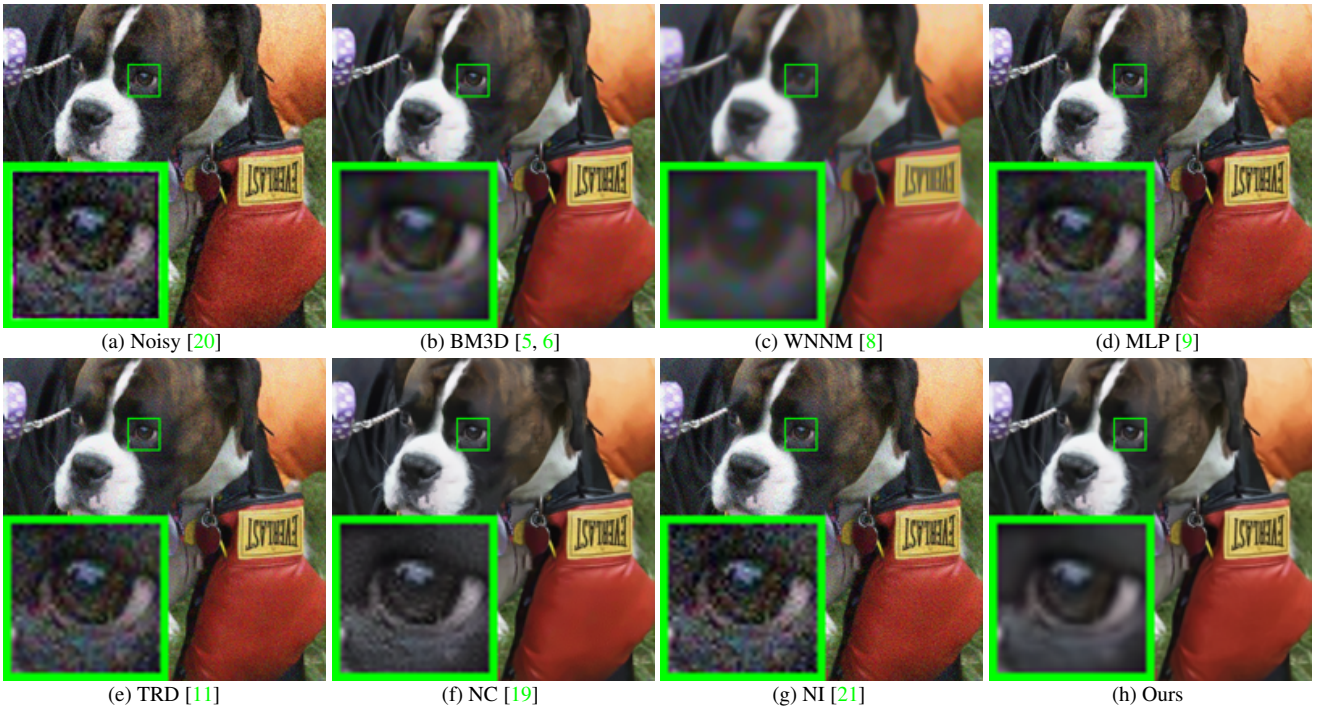


Figure 6. Denoised images of the real noisy image “Dog” by different methods. The images are better to be zoomed in on screen.

and TNRD are likely to remain many noise-caused color artifacts across the whole image. These results demonstrate that the methods designed with Gaussian noise model are not effective for real noise removal. Though NC and NI methods are specifically developed for real noisy images, their performance on noise removal is not very satisfactory. In comparison, our proposed method recovers much better the structures and textures (such as the eye area) than the other competing methods. More visual comparisons on dataset [20] can be found in the supplementary file.

#### 4.4.2 Comparison on Dataset [14]

As described in section 4.2, there is a mean image for each of the 17 scenes used in dataset [14], and those mean images can be roughly taken as “ground truth” images for quantitative evaluation of denoising algorithms. We firstly perform quantitative comparison on the 15 cropped images used in [14]. The PSNR results of CBM3D [5], WNNM [8], MLP [9], CSF [10], TNRD [11], NC [19] and CC [14] are listed in Table 3. (The results of CC are copied from the original paper [14].) The best PSNR result of each image is highlighted in bold. One can see that on 9 out of the 15 images, our method achieves the best PSNR values. CC achieves the best PSNR on 3 of the 15 images. It should be noted that in the CC method, a specific model is trained for each camera and camera setting, while our method uses the same model for all images. On average, our proposed method has 0.28dB PSNR improvements over [14] and much higher

Table 2. Average PSNR(dB) results of different methods on 60 real noisy images cropped from [14].

| Methods | <b>BM3D</b>  | <b>WNNM</b> | <b>MLP</b> | <b>CSF</b>   |
|---------|--------------|-------------|------------|--------------|
| PSNR    | 34.58        | 34.52       | 36.19      | 37.40        |
| Methods | <b>TRD</b>   | <b>NI</b>   | <b>NC</b>  | <b>Ours</b>  |
| PSNR    | <b>37.75</b> | 36.53       | 37.57      | <b>38.75</b> |

PSNR gains over other competing methods. Fig. ?? shows the denoised images of a scene captured by Canon 5D Mark 3 at ISO = 3200. We can see that CBM3D, WNNM, NC, NI, and CC would either remain noise or generate artifacts, while MLP, TNRD over-smooth much the image. By using the external prior guided internal priors, our proposed method preserves edges and textures better than other methods, leading to visually pleasant outputs. More visual comparisons can be found in the supplementary file.

We then perform denoising experiments on the 60 images we cropped from [14]. The average PSNR results are listed in Table 2 (CC is not compared since the code of [14] is not available). Again, our proposed method achieves much better PSNR results than the other methods. The improvement of our method over the second best method (TNRD) is about 1dB. Due to the space limitations, the visual comparisons are provided in the supplementary file.

## 5. Conclusion

The noise in real-world noisy images is much more complex than additive white Gaussian noise and hard to be mod-

Table 3. Average PSNR(dB) results of different methods on 15 cropped real noisy images used in [14].

| Camera Settings                 | Noisy | BM3D  | WNNM  | MLP   | CSF   | TRD   | NI    | NC    | CC    | Ours  |
|---------------------------------|-------|-------|-------|-------|-------|-------|-------|-------|-------|-------|
| Canon 5D Mark III<br>ISO = 3200 | 37.00 | 37.08 | 37.09 | 33.92 | 35.68 | 36.20 | 37.68 | 38.76 | 38.37 | 40.50 |
|                                 | 33.88 | 33.94 | 33.93 | 33.24 | 34.03 | 34.35 | 34.87 | 35.69 | 35.37 | 37.05 |
|                                 | 33.83 | 33.88 | 33.90 | 32.37 | 32.63 | 33.10 | 34.77 | 35.54 | 34.91 | 36.11 |
| Nikon D600<br>ISO = 3200        | 33.28 | 33.33 | 33.34 | 31.93 | 31.78 | 32.28 | 34.12 | 35.57 | 34.98 | 34.88 |
|                                 | 33.77 | 33.85 | 33.79 | 34.15 | 35.16 | 35.34 | 35.36 | 36.70 | 35.95 | 36.31 |
|                                 | 34.93 | 35.02 | 34.95 | 37.89 | 39.98 | 40.51 | 38.68 | 39.28 | 41.15 | 39.23 |
| Nikon D800<br>ISO = 1600        | 35.47 | 35.54 | 35.57 | 33.77 | 34.84 | 35.09 | 37.34 | 38.01 | 37.99 | 38.40 |
|                                 | 35.71 | 35.79 | 35.77 | 35.89 | 38.42 | 38.65 | 38.57 | 39.05 | 40.36 | 40.92 |
|                                 | 34.81 | 34.92 | 34.95 | 34.25 | 35.79 | 35.85 | 37.87 | 38.20 | 38.30 | 38.97 |
| Nikon D800<br>ISO = 3200        | 33.26 | 33.34 | 33.31 | 37.42 | 38.36 | 38.56 | 36.95 | 38.07 | 39.01 | 38.66 |
|                                 | 32.89 | 32.95 | 32.96 | 34.88 | 35.53 | 35.76 | 35.09 | 35.72 | 36.75 | 37.07 |
|                                 | 32.91 | 32.98 | 32.96 | 38.54 | 40.05 | 40.59 | 36.91 | 36.76 | 39.06 | 38.52 |
| Nikon D800<br>ISO = 6400        | 29.63 | 29.66 | 29.71 | 33.59 | 34.08 | 34.25 | 31.28 | 33.49 | 34.61 | 33.76 |
|                                 | 29.97 | 30.01 | 29.98 | 31.55 | 32.13 | 32.38 | 31.38 | 32.79 | 33.21 | 33.43 |
|                                 | 29.87 | 29.90 | 29.95 | 31.42 | 31.52 | 31.76 | 31.40 | 32.86 | 33.22 | 33.58 |
| Average                         | 33.41 | 33.48 | 33.48 | 34.32 | 35.33 | 35.65 | 35.49 | 36.43 | 36.88 | 37.16 |

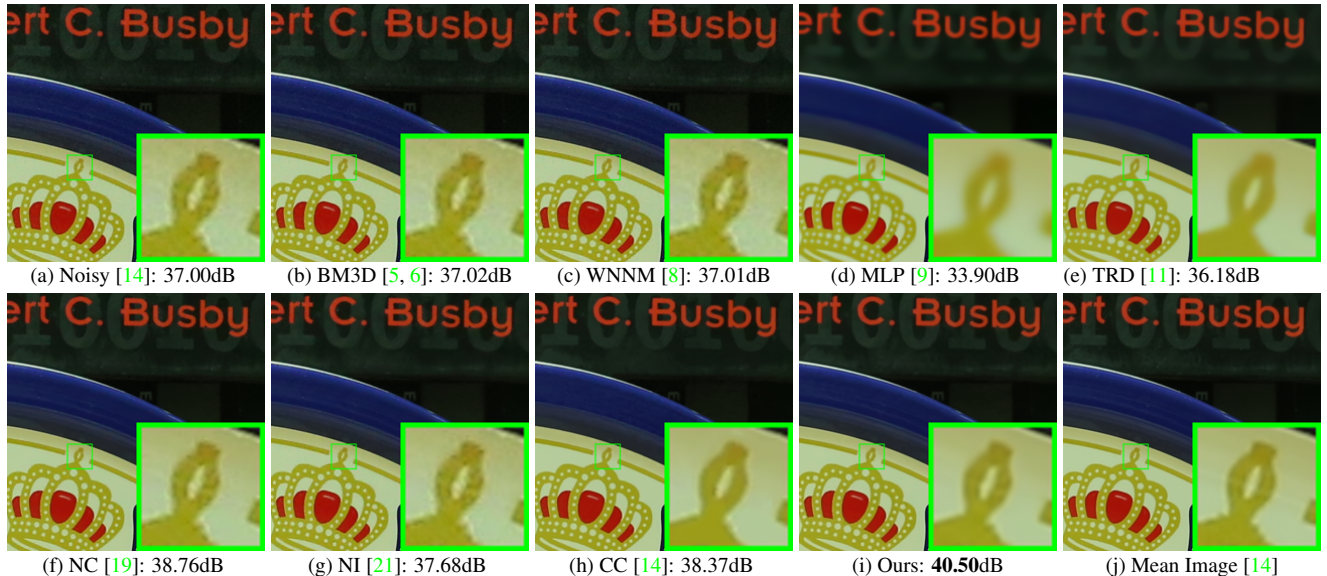


Figure 7. Denoised images of a noisy image cropped from the image “Canon 5D Mark 3 ISO 3200 1” by different methods. The images are better to be zoomed in on screen.

eled by simple analytical distributions such as Gaussian or mixture of Gaussians. In this paper, we proposed a simple yet effective solution for real noisy image denoising without explicitly assuming certain noise models. Specifically, we firstly learned image priors of Gausian Mixture Model from external clean images, and then employ the learned external priors to guide the learning of internal latent priors from the given noisy image. The learned hybrid orthogonal dictionary are simutaneously utilized in real noisy image denoising. Experiments on two real noisy image datasets, where the images were captured under indoor or outdoor lighting conditions by different types of cameras

and camera settings, demonstrate that our proposed method achieved much better performance than state-of-the-art image denoising methods.

## References

- [1] M. Elad and M. Aharon. Image denoising via sparse and redundant representations over learned dictionaries. *IEEE Transactions on Image Processing*, 15(12):3736–3745, 2006. 1, 2
- [2] J. Mairal, F. Bach, J. Ponce, G. Sapiro, and A. Zisserman. Non-local sparse models for image restoration. *IEEE International Conference on Computer Vision (ICCV)*, pages 2272–2279, 2009. 1

- 864 [3] W. Dong, L. Zhang, G. Shi, and X. Li. Nonlocally central- 918  
865 ized sparse representation for image restoration. *IEEE Trans- 919  
866 actions on Image Processing*, 22(4):1620–1630, 2013. 1, 2, 920  
867 6  
868 [4] A. Buades, B. Coll, and J. M. Morel. A non-local algorithm 921  
869 for image denoising. *IEEE Conference on Computer Vision 922  
870 and Pattern Recognition (CVPR)*, pages 60–65, 2005. 1  
871 [5] K. Dabov, A. Foi, V. Katkovnik, and K. Egiazarian. Image 923  
872 denoising by sparse 3-D transform-domain collabora- 924  
873 tive filtering. *IEEE Transactions on Image Processing*, 925  
874 16(8):2080–2095, 2007. 1, 2, 5, 6, 7, 8  
875 [6] K. Dabov, A. Foi, V. Katkovnik, and K. Egiazarian. Color 926  
876 image denoising via sparse 3D collaborative filtering with 927  
877 grouping constraint in luminance-chrominance space. *IEEE 928  
878 International Conference on Image Processing (ICIP)*, pages 929  
879 313–316, 2007. 1, 2, 5, 6, 7, 8  
880 [7] J. Xu, L. Zhang, W. Zuo, D. Zhang, and X. Feng. Patch 930  
881 group based nonlocal self-similarity prior learning for image 931  
882 denoising. *IEEE International Conference on Computer Vi- 932  
883 sion (ICCV)*, pages 244–252, 2015. 1, 2, 3, 5  
884 [8] S. Gu, L. Zhang, W. Zuo, and X. Feng. Weighted nu- 933  
885 clear norm minimization with application to image denois- 934  
886 ing. *IEEE Conference on Computer Vision and Pattern 935  
887 Recognition (CVPR)*, pages 2862–2869, 2014. 1, 2, 5, 6, 936  
888 7, 8  
889 [9] H. C. Burger, C. J. Schuler, and S. Harmeling. Image 937  
890 denoising: Can plain neural networks compete with BM3D? 938  
891 *IEEE Conference on Computer Vision and Pattern Recog- 939  
892 nition (CVPR)*, pages 2392–2399, 2012. 1, 2, 5, 6, 7, 8  
893 [10] U. Schmidt and S. Roth. Shrinkage fields for effective image 940  
894 restoration. *IEEE Conference on Computer Vision and Pat- 941  
895 tern Recognition (CVPR)*, pages 2774–2781, June 2014. 1, 942  
896 2, 5, 6, 7  
897 [11] Y. Chen, W. Yu, and T. Pock. On learning optimized re- 943  
898 action diffusion processes for effective image restoration. 944  
899 *IEEE Conference on Computer Vision and Pattern Recog- 945  
900 nition (CVPR)*, pages 5261–5269, 2015. 1, 2, 5, 6, 7, 8  
901 [12] S. Roth and M. J. Black. Fields of experts. *International 946  
902 Journal of Computer Vision*, 82(2):205–229, 2009. 1, 2  
903 [13] D. Zoran and Y. Weiss. From learning models of natural 947  
904 image patches to whole image restoration. *IEEE Interna- 948  
905 tional Conference on Computer Vision (ICCV)*, pages 479– 949  
906 486, 2011. 1, 2, 3  
907 [14] S. Nam, Y. Hwang, Y. Matsushita, and S. J. Kim. A holistic 950  
908 approach to cross-channel image noise modeling and its ap- 951  
909 plication to image denoising. *IEEE Conference on Computer 952  
910 Vision and Pattern Recognition (CVPR)*, pages 1683–1691, 953  
911 2016. 1, 2, 5, 6, 7, 8  
912 [15] G. E Healey and R. Kondepudy. Radiometric CCD cam- 954  
913 era calibration and noise estimation. *IEEE Transactions on 955  
914 Pattern Analysis and Machine Intelligence*, 16(3):267–276, 956  
915 1994. 1  
916 [16] C. Liu, R. Szeliski, S. Bing Kang, C. L. Zitnick, and W. T. 957  
917 Freeman. Automatic estimation and removal of noise from 958  
918 a single image. *IEEE Transactions on Pattern Analysis and 959  
919 Machine Intelligence*, 30(2):299–314, 2008. 1, 2  
920 [17] Z. Gong, Z. Shen, and K.-C. Toh. Image restoration with 921  
921 mixed or unknown noises. *Multiscale Modeling & Simula- 922  
922 tion*, 12(2):458–487, 2014. 1, 2  
923 [18] F. Zhu, G. Chen, and P.-A. Heng. From noise modeling to 924  
924 blind image denoising. *IEEE Conference on Computer Vi- 925  
925 sion and Pattern Recognition (CVPR)*, June 2016. 1, 2  
926 [19] M. Lebrun, M. Colom, and J.-M. Morel. Multiscale image 927  
927 blind denoising. *IEEE Transactions on Image Processing*, 928  
928 24(10):3149–3161, 2015. 1, 2, 5, 6, 7, 8  
929 [20] M. Lebrun, M. Colom, and J. M. Morel. The noise clinic: 930  
930 a blind image denoising algorithm. [http://www.ipol.](http://www.ipol.im/pub/art/2015/125/) 931  
931 [im/pub/art/2015/125/](http://www.ipol.im/pub/art/2015/125/). Accessed 01 28, 2015. 1, 2, 932  
932 5, 6, 7  
933 [21] Neatlab ABSoft. Neat Image. [https://ni.](https://ni.neatvideo.com/home) 934  
934 [neatvideo.com/home](https://ni.neatvideo.com/home). 1, 2, 5, 6, 7, 8  
935 [22] G. Yu, G. Sapiro, and S. Mallat. Solving inverse problems 936  
936 with piecewise linear estimators: From Gaussian mixture 937  
937 models to structured sparsity. *IEEE Transactions on Image 938  
938 Processing*, 21(5):2481–2499, 2012. 2  
939 [23] M. Zontak and M. Irani. Internal statistics of a single natural 940  
940 image. *IEEE Conference on Computer Vision and Pattern 941  
941 Recognition (CVPR)*, pages 977–984, 2011. 2  
942 [24] M. Lebrun, A. Buades, and J. M. Morel. A nonlocal 943  
943 Bayesian image denoising algorithm. *SIAM Journal on 944  
944 Imaging Sciences*, 6(3):1665–1688, 2013. 2  
945 [25] D. L. Donoho and X. Huo. Uncertainty principles and ideal 946  
946 atomic decomposition. *IEEE Transactions on Information 947  
947 Theory*, 47(7):2845–2862, 2001. 4  
948 [26] H. Zou, T. Hastie, and R. Tibshirani. Sparse principal 949  
949 component analysis. *Journal of Computational and Graphical 950  
950 Statistics*, 15(2):265–286, 2006. 4  
951 [27] X. Liu, M. Tanaka, and M. Okutomi. Single-image noise 952  
952 level estimation for blind denoising. *IEEE transactions on 953  
953 Image Processing*, 22(12):5226–5237, 2013. 6  
954 [28] S. Nam, Y. Hwang, Y. Matsushita, and S. J. Kim. A holistic 955  
955 approach to cross-channel image noise modeling and its ap- 956  
956 plication to image denoising. *IEEE Conference on Computer 957  
957 Vision and Pattern Recognition (CVPR)*, pages 1683–1691, 958  
958 2016. 1, 2, 5, 6, 7, 8  
959 [29] G. E Healey and R. Kondepudy. Radiometric CCD cam- 959  
959 era calibration and noise estimation. *IEEE Transactions on 960  
960 Pattern Analysis and Machine Intelligence*, 16(3):267–276, 961  
961 1994. 1  
962 [30] C. Liu, R. Szeliski, S. Bing Kang, C. L. Zitnick, and W. T. 962  
962 Freeman. Automatic estimation and removal of noise from 963  
963 a single image. *IEEE Transactions on Pattern Analysis and 964  
964 Machine Intelligence*, 30(2):299–314, 2008. 1, 2  
965 [31] Z. Gong, Z. Shen, and K.-C. Toh. Image restoration with 965  
965 mixed or unknown noises. *Multiscale Modeling & Simula- 966  
966 tion*, 12(2):458–487, 2014. 1, 2  
967 [32] F. Zhu, G. Chen, and P.-A. Heng. From noise modeling to 967  
967 blind image denoising. *IEEE Conference on Computer Vi- 968  
968 sion and Pattern Recognition (CVPR)*, June 2016. 1, 2  
969 [33] M. Lebrun, M. Colom, and J. M. Morel. Multiscale image 969  
969 blind denoising. *IEEE Transactions on Image Processing*, 970  
970 24(10):3149–3161, 2015. 1, 2, 5, 6, 7, 8  
971